800 MEV RF STRUCTURES*

E. Knapp
Los Alamos Scientific Laboratory, University of California
Los Alamos, New Mexico

I would first like to say that the people who have been working on this are Bruce Knapp, Bill Shlaer, Jim Potter and myself. This report is certainly that of a joint effort.

For the successful construction of a high energy proton linear accelerator, an rf structure which provides an electromagnetic wave traveling with the velocity of the accelerating proton, which is insensitive to beam level in the accelerator, is easily monitored and controlled by the driving amplifier, and which has a minimum of power loss in its walls is necessary. It appears that a chain of cavities operating as a resonant structure, whose lengths are adjusted to provide the changing phase velocity required for the acceleration, best fulfills the above requirements. Due to the resonant cavity nature of the system, the axial dependence of the amplitude of the accelerating wave is not cirtically dependent on beam level as it would be in a traveling wave accelerator. It also has been possible to obtain structures which have good shunt impedances in a resonant mode and thus fulfill the efficiency requirement mentioned above.

Many structures which may be operated in π-mode have been proposed as accelerator elements. Among the possibilities are 1) an iris-loaded structure such as is used in a traveling wave application in the Stanford linear electron accelerators, 2) a crossed-bar structure suggested by Walkinshaw at Harwell and investigated by A. Carne there, 3) the cloverleaf structure discussed by Chodorow and Craig and investigated by A. Carne at Harwell, 4) a basket-weave structure such as has been suggested by Chodorow and Craig, 5) alternatively a set of loop-coupled pill-box cavities as have been discussed by the Harwell group, 6) modifications of many of the traveling wave amplifier tube structures, such as slow wave helices, which have been used successfully in that application. Structures which basically operate in the $\pi/2$ mode (resonant coupling, are also considered in this paper. Some work has been done on structures with resonant coupling loops by the Harwell group. A series of measurements on model cavities of the above types has been undertaken in order to choose a structure for use in the proposed linear accelerator meson facility at Los Alamos. In the following we will discuss in detail

*Work performed under the auspices of the U. S. Atomic Energy Commission.

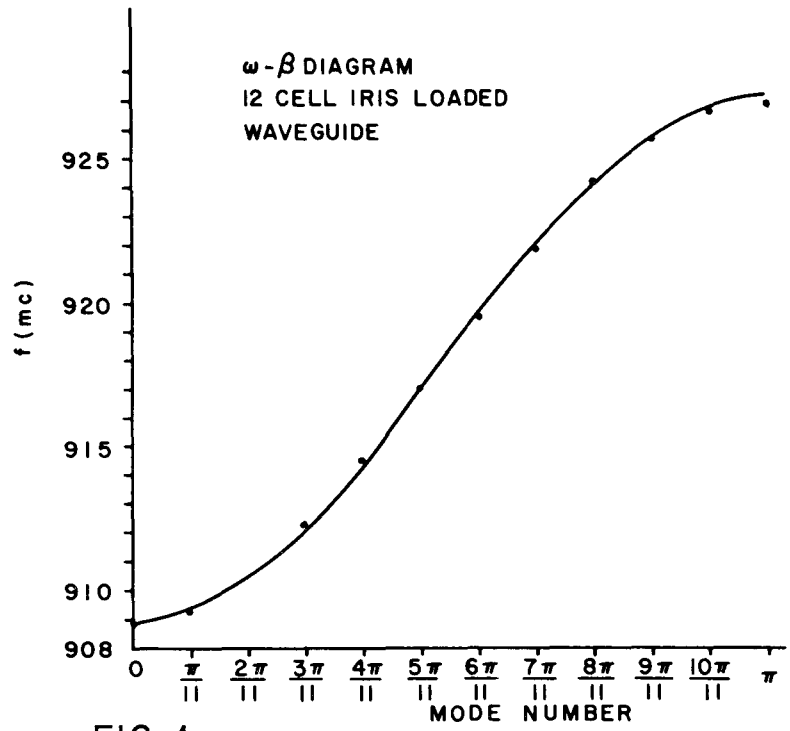
ω - β DIAGRAM
12 CELL IRIS LOADED
WAVEGUIDE
f (mc)
925
920
915
910
908
0
π/11
2π/11
3π/11
4π/11
5π/11
6π/11
7π/11
8π/11
9π/11
10π/11
π
MODE NUMBER

FIG. 1

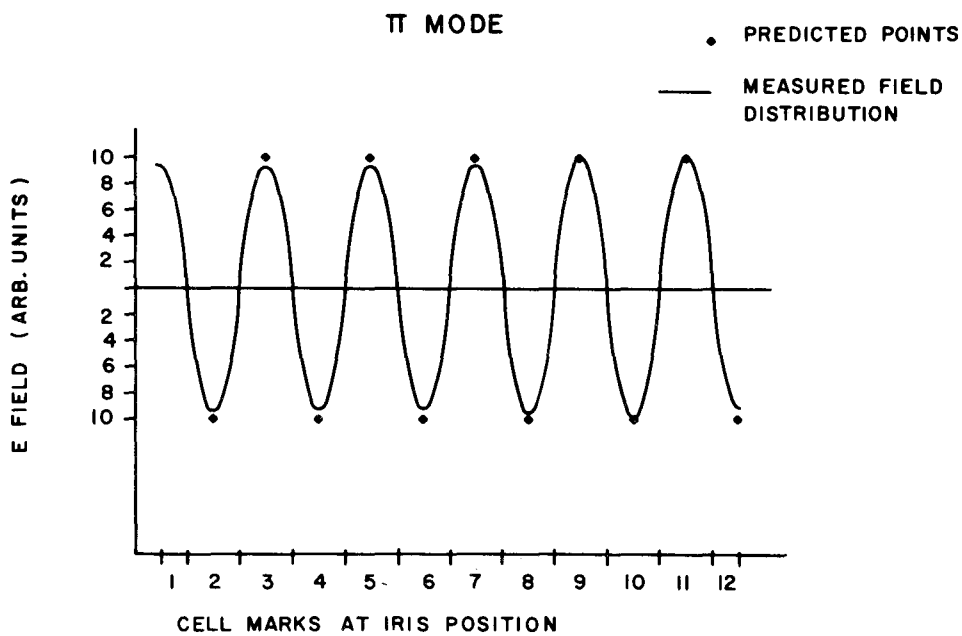
π MODE
PREDICTED POINTS
MEASURED FIELD
DISTRIBUTION
E FIELD (ARB. UNITS)
10
8
6
4
2
2
4
6
8
10
1 2 3 4 5 6 7 8 9 10 11 12
CELL MARKS AT IRIS POSITION

FIG. 2

the cloverleaf structure mentioned above, and a possible $\pi/2$ mode configuration which exhibits good shunt impedance.

Electrical Properties of N Coupled Cavities

The electrical properties of n magnetically coupled lumped constant resonant circuits may be taken as a guide to the properties of n coupled cavities, with the appropriate identification of properties of the circuits to characteristics of the cavities. Such an analysis has been carried out and has been described in the previous paper. If there are N cells or cavities coupled together with a mutual inductance $M = k L$ where L is the self-inductance in each loop of the equivalent circuit, then there will be N resonant frequencies for the circuit as a whole, distributed in frequency as

$$1 - \frac{\omega_o^2}{\omega^2} + k \cos \phi = 0 \qquad (1)$$

where ω_o = individual cell frequency. The circulating currents in the individual loops have amplitudes

$$i_n = \cos \frac{\pi q n}{N} ,$$

where n is the cell number and q the mode number. In π mode for a lossless case (q = N) all currents are equal, there is a π phase change from cell to cell, and the separation of the $\frac{(N-1)}{N}\pi$ mode from the π mode is

$$\frac{\Delta\omega}{\omega_o} = \frac{k \pi^2}{4 N^2}$$

for $k << 1$. Cleraly the coupling from cell to cell must be made as great as possible in order to keep good mode separation. If there are losses in the individual circuits, the phase change from cell to cell is no longer π, but $\pi - \Delta\phi$ where

$$\phi_{n, n+1} = \frac{2 (1 - k)}{k Q} \left(n + \frac{1}{2} \right)$$

or the phase shift across n cells is

$$\phi_{o, n} = \frac{(1 - k)}{k Q} n^2 \qquad (3)$$

where n = 0 is the cell furthest from the drive and the numbering is toward the cell into which energy is introduced. In order to keep the phase velocity of the accelerating wave correct, $\Delta\phi$ must not change appreciably with beam level, which means k must be as high as possible. Finally, in order to be able to effectively tune or flatten the tank, the theory also indicates k must be as large as possible. First-order perturbation theory indicates that the amplitude error associated with a frequency error distribution

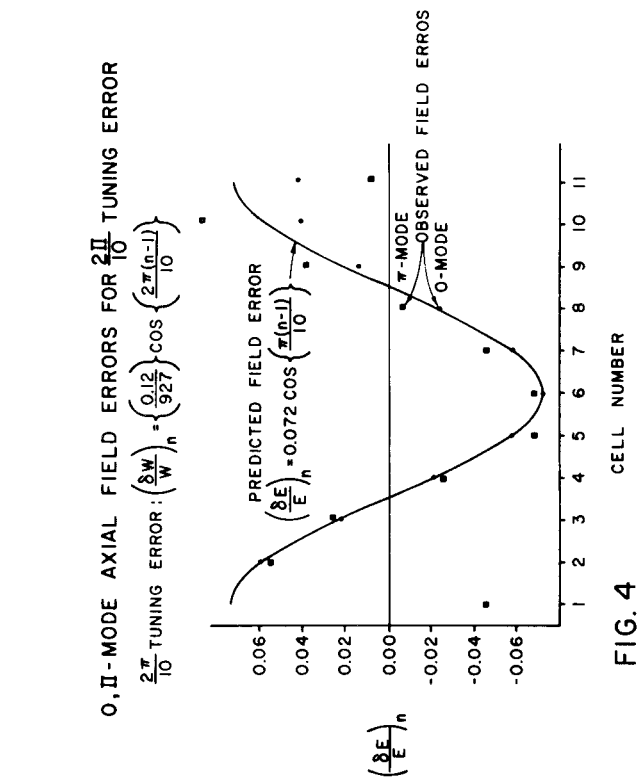

FIG. 4

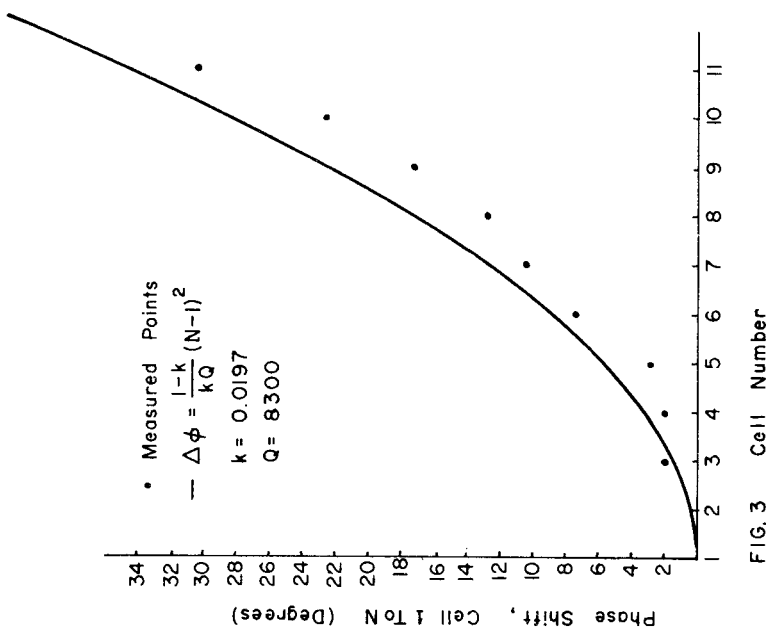

FIG. 3 Cell Number

$$\tilde{\epsilon}_r = \frac{2\,W(r)}{N} \sum_{p=0}^{N} W(p)\ \epsilon_p \cos\frac{\pi pr}{N} \tag{4}$$

where $W(p) = \frac{1}{2}$, $p = 0, N$

$W(p) = 1$, $p \neq 0, N$

$$\epsilon_p = \left(\frac{\omega_{op}^2 - \omega_o^2}{\omega_o^2} \right)_{p^{th}\ \text{cell}}$$

is

$$\delta i_n^q = \sum_{r=1}^{N} \tilde{\epsilon}_r \frac{1}{2} \left\{ \frac{W(q-r)}{W(r)}\ a_r \cos\frac{\pi(q+r)n}{N} + \frac{W(q+r)}{W(r)}\ a_{-r} \cos\frac{\pi(q-r)n}{N} \right\} \tag{5}$$

where $a_r = \left\{ \left(\frac{\omega_o}{\omega_{q+r}} \right)^2 - \left(\frac{\omega_o}{\omega_q} \right)^2 \right\}^{-1}$.

For a π mode

$$\frac{\delta I_n^N}{I_n^N} = \frac{1}{k} + \sum_{r=1}^{N} \tilde{\epsilon}_r \frac{\cos\frac{\pi rn}{N}}{1 - \cos\frac{\pi r}{N}} \tag{6}$$

and for $\pi/2$ mode we have

$$\frac{\delta I_n^{n/2}}{I_o^{N/2}} = -\frac{1}{k} \sum_{r=1}^{N} \tilde{\epsilon}_r \frac{W(N/2 - r)}{\sin\frac{\pi r}{N}} \sin\frac{\pi n}{2} \sin\frac{\pi rn}{N}. \tag{7}$$

These relationships have been verified for a 12-cell iris-loaded cavity to better than 5% accuracy. Here k is identified with the bandwidth of the structure

$$k = \frac{\omega_{(\pi)} - \omega_{(o)}}{\omega_{AVE}}$$

as would be indicated by Eq. (1). The current in Eq. (2) has been experimentally identified with the electric field at the center of individual cells.

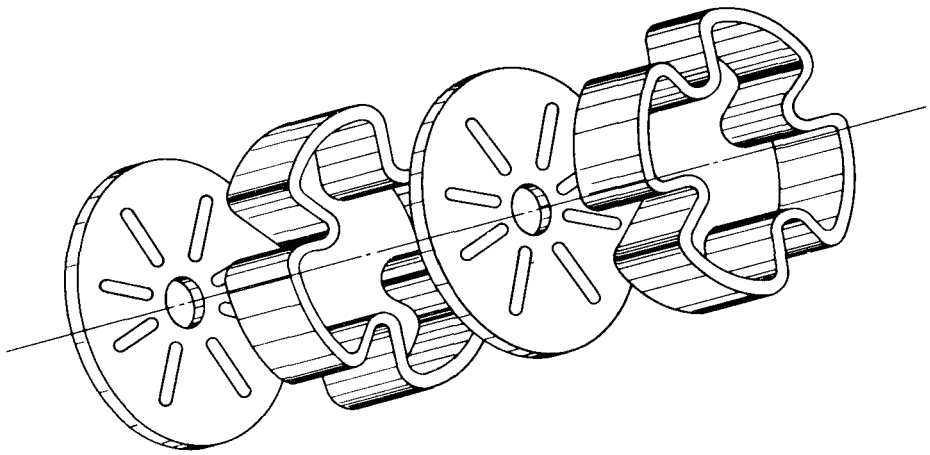

800 MEGACYCLE
CLOVERLEAF COMPONENTS

FIG. 5

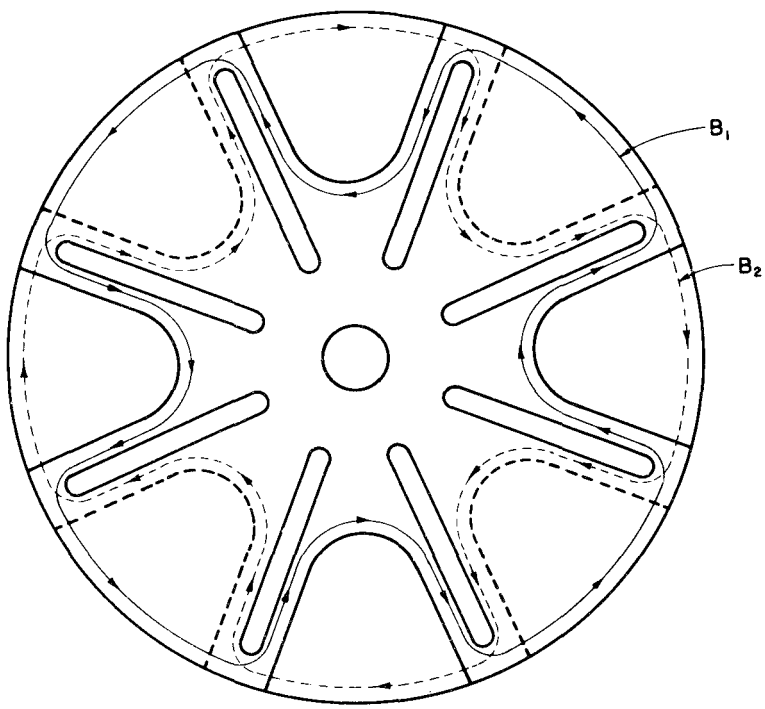

FIG. 6

Figure 1 shows the dispersion curve for a 12-cell iris-loaded waveguide resonator, compared to the predicted curve for k = 0.0197. Figure 2 shows the predicted center cell amplitudes vs measured field distributions for the π mode in the structure. Figure 3 shows the measured phase shift vs predicted phase shift for Q = 8300. Figure 4 shows a comparison of the measured and predicted ampltiude distributions for programmed tuning errors in the cavities.

The above theory suffices for an iris-loaded waveguide. However, in many instances the coupling mechanism itself may have resonances near the cavity resonant frequency. For this reason we have considered a chain of coupled resonators as before, but now alternating with frequencies ω_1 and ω_2, as also described in the previous paper. We then find a dispersion relation

$$\left(\omega^2 - \omega_1^2\right)\left(\omega^2 - \omega_2^2\right) = \omega^4 K^2 \cos^2 \phi \qquad (8)$$

where now ϕ is the phase change from cell to slot, say, and K is identified with the coupling of slot to cell. K may be identified with the full passband width if $\omega_1 = \omega_2$. The dispersion curve for a structure of this type displays a stop band as discussed in the previous paper. While the behavior of a chain of circuits such as this is somewhat more complex for the general case, an effective coupling constant k_{eff} may be defined to allow use of the single resonant frequency theory of phase shifts near the $\pi/2$ mode of the multiply resonant structures. This coupling constant may be defined by making a Taylor expansion of the dispersion curve near the $\pi/2$ mode for the multiply-periodic circuit and matching this to a symmetric dispersion curve as obtained in the theory for a chain of resonant cavities with a single resonant frequency. Carrying this out we find that

$$k = \frac{K^2}{2(P-1) + K^2} \qquad (9)$$

where $P = \omega_1^2 / \omega_2^2$.

The validity of this approximation has been investigated for the phase shift problem with computer runs and on experimental models and agrees very well with the observed results. For the perturbation theory, agreement with experiment seems excellent also.

In general, we find k's considerably bigger than the measured bandwidth, which would intuitively be the case since the dispersion curves are quite asymmetric. We shall refer to these expressions often as we describe the experimental results obtained.

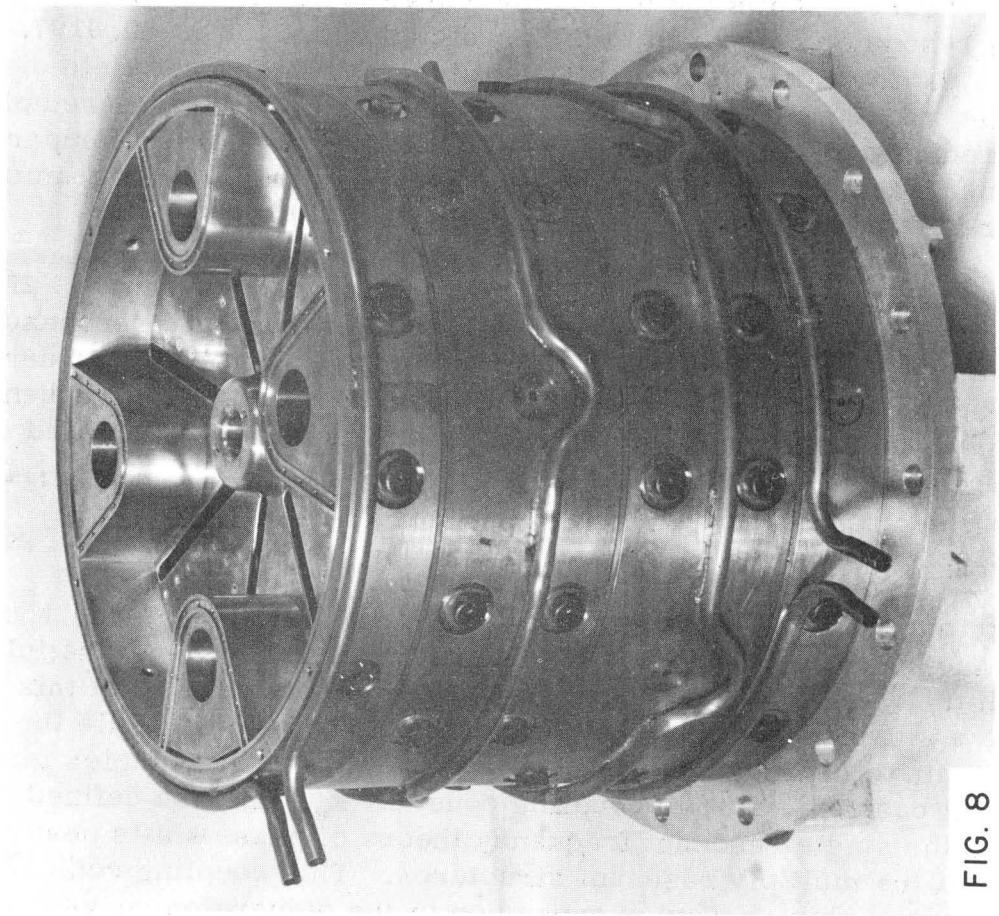

FIG. 8

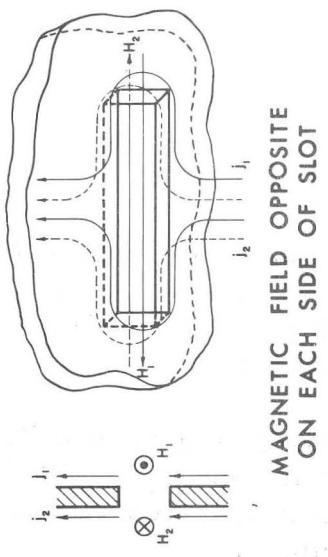
MAGNETIC FIELD OPPOSITE
ON EACH SIDE OF SLOT

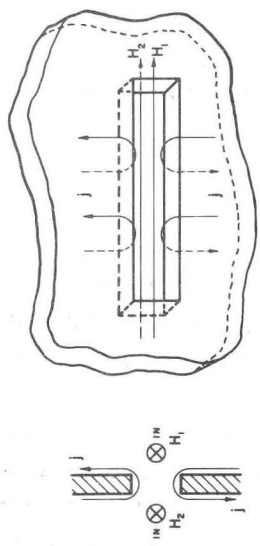
MAGNETIC FIELD IN SAME DIRECTION
ON EACH SIDE OF SLOT

FIG. 7

Accelerator Efficiency

The efficiency of a resonant cavity as a particle accelerating device may be measured by considering the power required to provide a given acceleration; it is usually expressed in terms of the effective shunt impedance

$$ZT^2 = \frac{(\text{energy gain/meter})^2}{\text{power dissipated/meter}} = \frac{\text{ohms}}{\text{meter}}$$

where the energy gain is taken for a particle located in the center of the accelerating gap at peak electric field.

$$ZT^2 = \frac{\left(\int E(z,t)\,dz\right)^2}{P\,L} \qquad (10)$$

where P = power dissipated in cavity, L = cavity length, and the integral is taken with the particle at the center of the cell at peak field.

The two most important criteria to be met by a π mode accelerating structure are that it have a large bandwidth (large k), and that the shunt impedance ZT^2 be as great as possible. In addition to these two criteria, it is reasonable also to expect the structure to develop no large electric fields in the mechanism used for coupling from cell to cell and not to present unsurmountable alignment or fabrication problems.

Structures Considered

Most of the mentioned type structures have been at least given a cursory examination with models using reasonable geometrical parameters. However, we have defined our principal investigation to two structures which look most promising to us, the cloverleaf π-mode structure and a version of a $\pi/2$ mode structure. Other laboratories are investigating most of the other structures more thoroughly than we could, so we will not comment on our results with these structures at this time.

CLOVERLEAF STRUCTURE

Historically the cloverleaf structure was invented for a traveling wave tube application by Chodorow and Craig and has been used commercially (Varian Assoc.) as an active element in a high power S-band traveling wave tube (types VA 125, VA 126, VA 145). Tube type VA 145 amplifies to 7 MW peak over an 8% bandwidth near 3 kMc. Other commercial tubes may be available of which we are not aware.

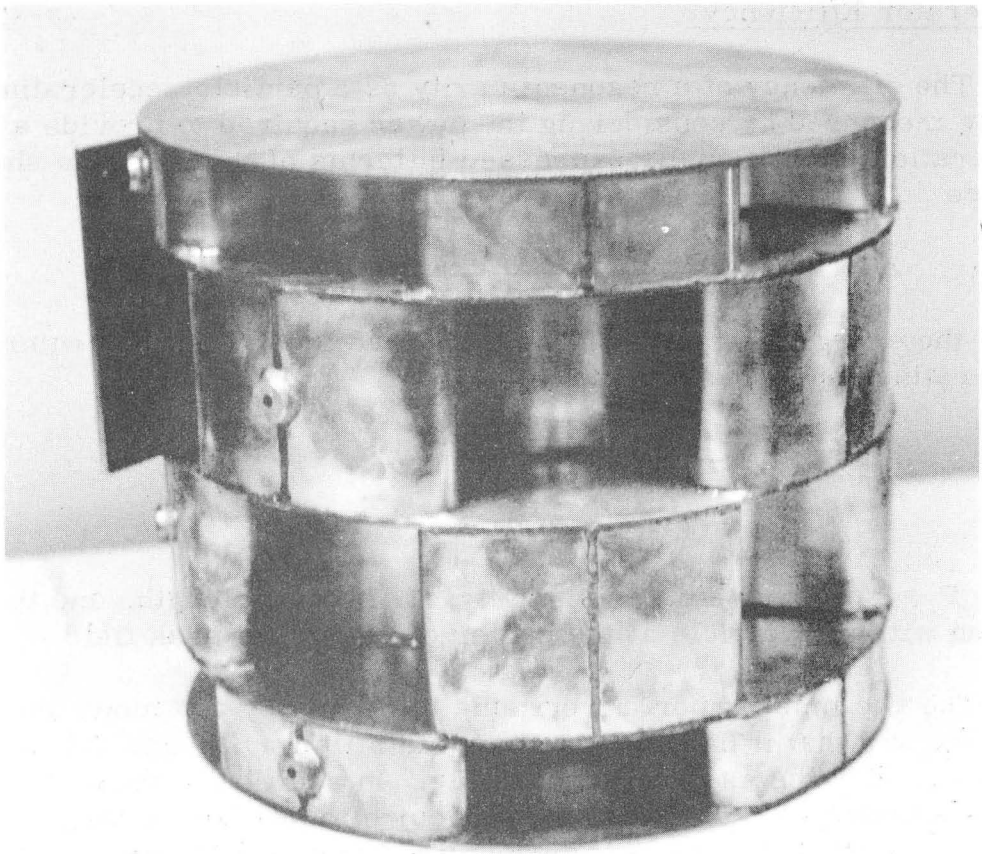

FIG. 9

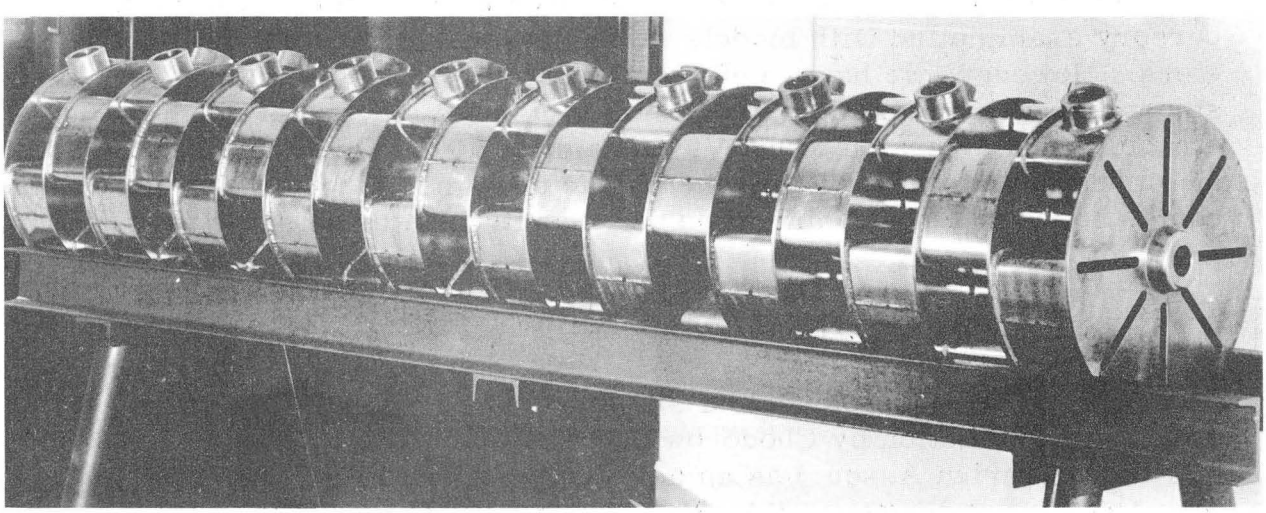

FIG. 10

Alan Carne from the Rutherford Laboratory has reported some studies on this structure as a possible element for a proton linear accelerator (Dubna Conference), and it was these measurements which drew our attention to this structure. As far as we know, no other measurements have been made for proton accelerator application of this structure.

Figure 5 shows an exploded view of the cloverleaf chain as envisioned by Chodorow and Craig. The periodicity operation in the cloverleaf is a translation by a cell length **L** and a rotation by 45°, as is indicated in more detail in Fig. 6.

Electromagnetically, the cloverleaf operates qualitatively as follows: Radial magnetic field lines are produced in the TM_{010} mode of a cylinder by deformations or noses in the walls of a cylindrical cavity at 90° intervals around its circumference. These radial fields may then be used to efficiently couple energy from one cell of the cloverleaf to the next by placing slots along these field lines. Eight slots are radially placed at 45° intervals straddling the noses protruding into the volume. On the other side of the septum we may have a 45° rotation of the cavity (forward wave structure) or 0° rotation of the structure (backward wave structure). For use as a standing wave accelerator structure, it is immaterial whether the structure is forward or backward wave. However, slot field levels and effective coupling strengths are important, and these are both favorable in the forward wave configuration for π-mode operation. In π mode with 45° rotation of the noses the radial fields are in the same direction on both sides of the slot. Figure 7 illustrates the current configurations near the slots in the cloverleaf for the zero mode (magnetic field opposite across slot) and π mode (magnetic field in same direction on each side of slot) in the forward wave configuration. The wall currents are clearly strongly perturbed in the zero mode and virtually unperturbed in the π mode, indicating a lowering of the zero mode frequency relative to that of the π mode (forward wave structure), and indicating that in π mode very little electric field will be developed across the slot. Energy transfer may be considered as a current interchange through the slot with almost no perturbation of the cavity mode fields in the process. The advantages we see in the cloverleaf as a standing wave accelerator structure are:

1. Coupling not dependent on beam aperture configuration.
2. Strong coupling available in π mode standing wave operation.
3. No strong electric fields present in coupling mechanisms.
4. Excellent shunt impedance possible, especially with capacitive loading in the cavities.

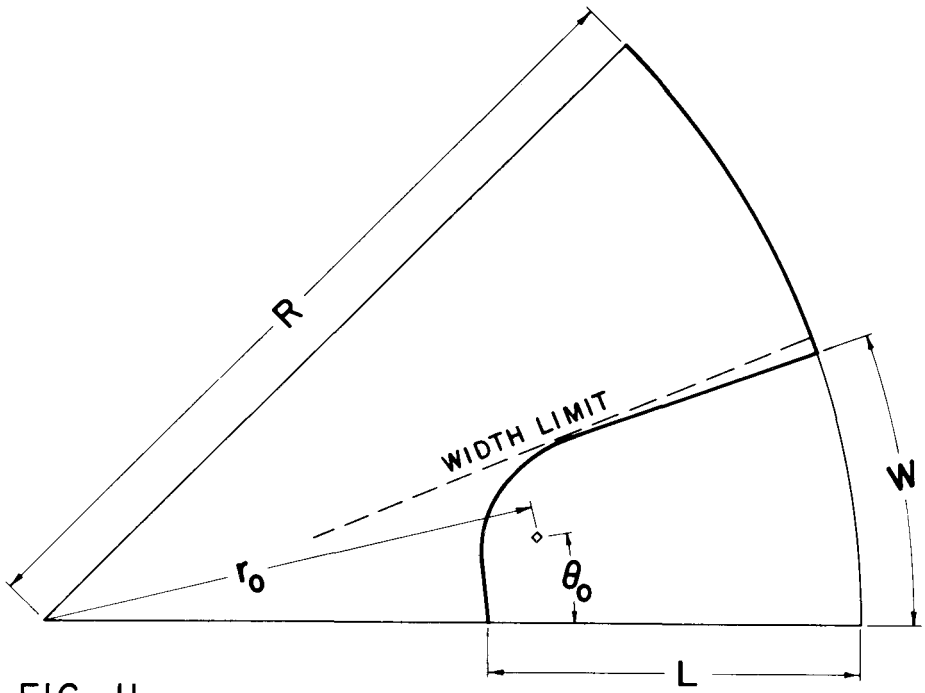
R
WIDTH LIMIT
W
r_o
θ_o
L

FIG. 11

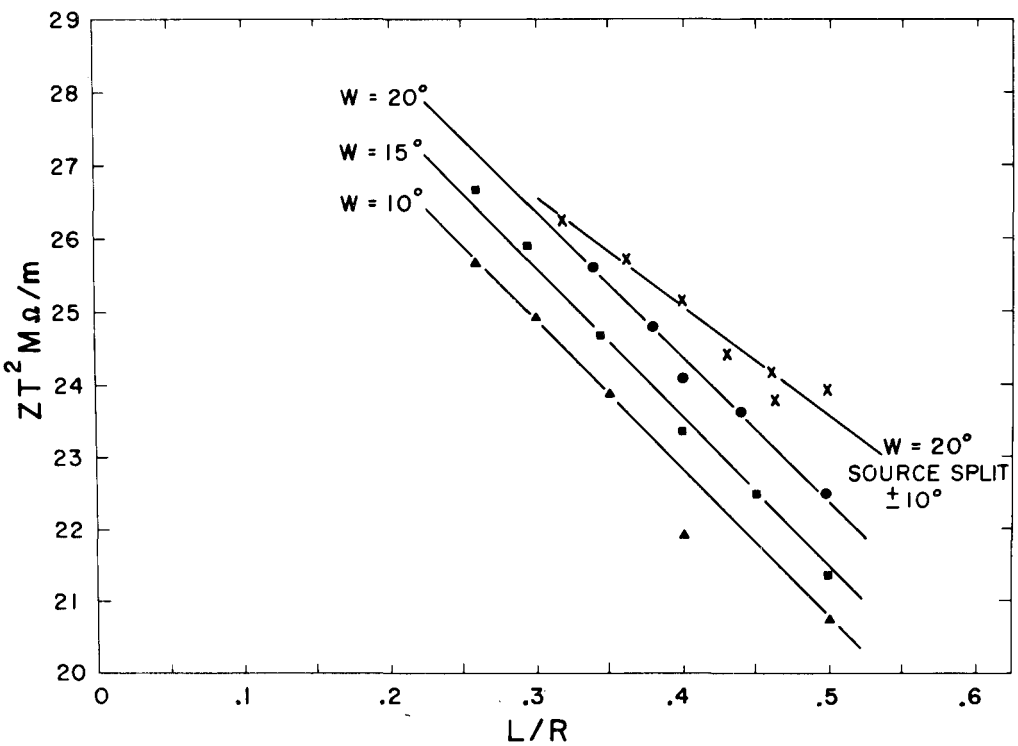
29
28
27
26
25
24
23
22
21
20
$ZT^2 M\Omega/m$
0
.1
.2
.3
.4
.5
.6
L/R
W = 20°
W = 15°
W = 10°
W = 20°
SOURCE SPLIT
±10°

FIG. 12

In order to investigate the properties of the cloverleaf more fully, we have constructed several models and measured their properties. Figure 8 shows a photograph of a demountable carefully machined model on which most of the optimizing studies have been done. This model allows the septum configuration to be changed at will, allowing studies of slot dimensions, beam hole size and configuration, and so on to be made. This model does not allow changes to be made in nose dimension. Also this model, because of its demountable joints, does not allow reliable Q measurements to be made; however, Z/Q measurements are quite reliable.

In order to make reliable Q measurements, several models were made up of two cells and two half cells (similar to the demountable configuration) in which all joints were brazed. These were manufactured by pressing 1/16-inch copper sheet in quadrants to form the cloverleaf walls, and heli-arc brazing the parts together with Sil-Fos solder. Using this same technique several single cell cloverleaf cavities were constructed also. Figure 9 shows a representative cavity of this type.

Figure 10 shows a 21-cell tank made by the same technique as above. This tank has been designed rather conservatively and has been used so far to check out the results of the shorter model studies and the predictions of the coupled circuit theory.

OPTIMIZATION OF NOSE SHAPE

Bill Shlaer at this laboratory has developed a computational program that allows calculation of electric and magnetic fields in a resonator similar to the cloverleaf. The fields in these resonators are generated by line currents oscillating at 800 Mc and located symmetrically in quadrants of a metal cylinder. The fields are assumed z-independent. In many respects this calculation is similar to that done by R. Gluckstern for drift tube and iris structures. Figure 11 shows the configuration of line currents (shown at position r_o and θ_o in an octant). The resultant fields may be varied by varying the cylinder radius and source radius. For certain ranges of these parameters, there is a zero of the electric field along which a new boundary may be drawn that will separate the currents from the rest of the cylinder. This remainder is resonant at 800 Mc with the same field distribution and may have the shape of a cloverleaf. These calculations do not include slots, beam holes, or any z-asymmetries. However, they do allow optimization of lobe shape for a given lobe penetration. Figure 12 shows shunt impedances calculated vs nose penetration L/R with nose width as a parameter. One family of flat-nosed lobes is included. It appears that for minimum losses, flat-nosed lobes are to be preferred with maximum width possible. These

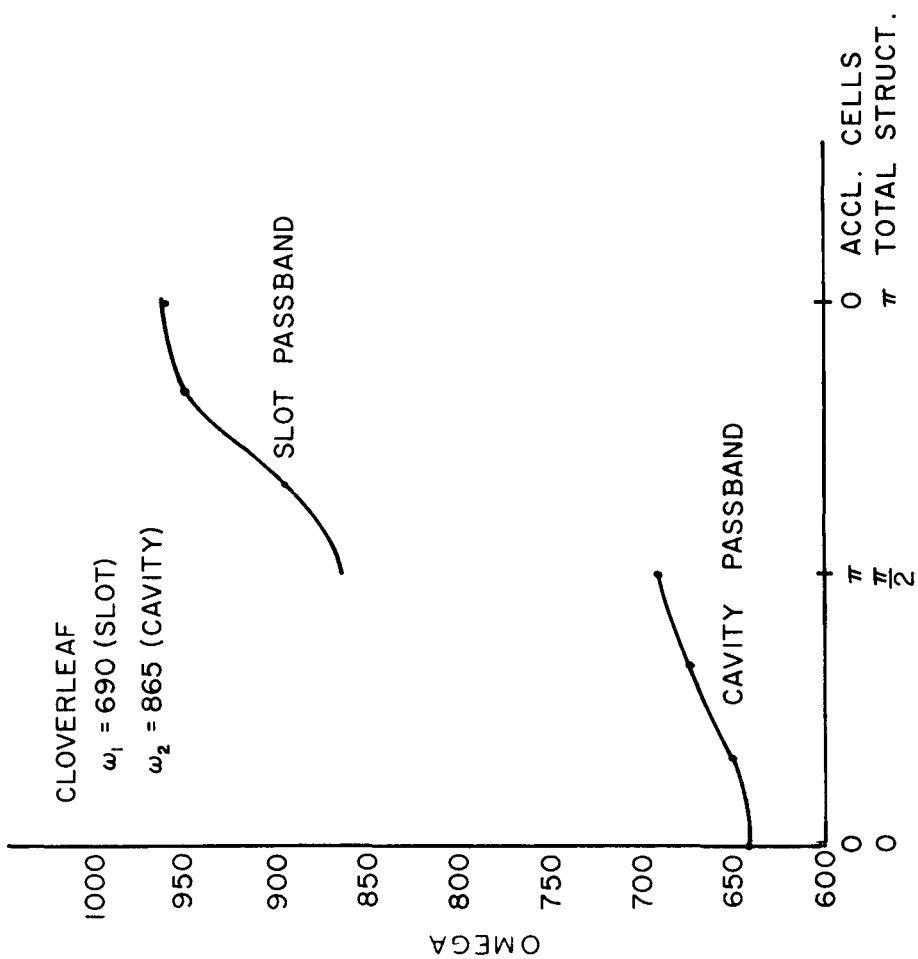
CLOVERLEAF
ω_1 = 690 (SLOT)
ω_2 = 865 (CAVITY)
SLOT PASSBAND
CAVITY PASSBAND
OMEGA
1000
950
900
850
800
750
700
650
600
0
$\frac{\pi}{2}$
π
0 ACCL. CELLS
π TOTAL STRUCT.
MODE

FIG. 14

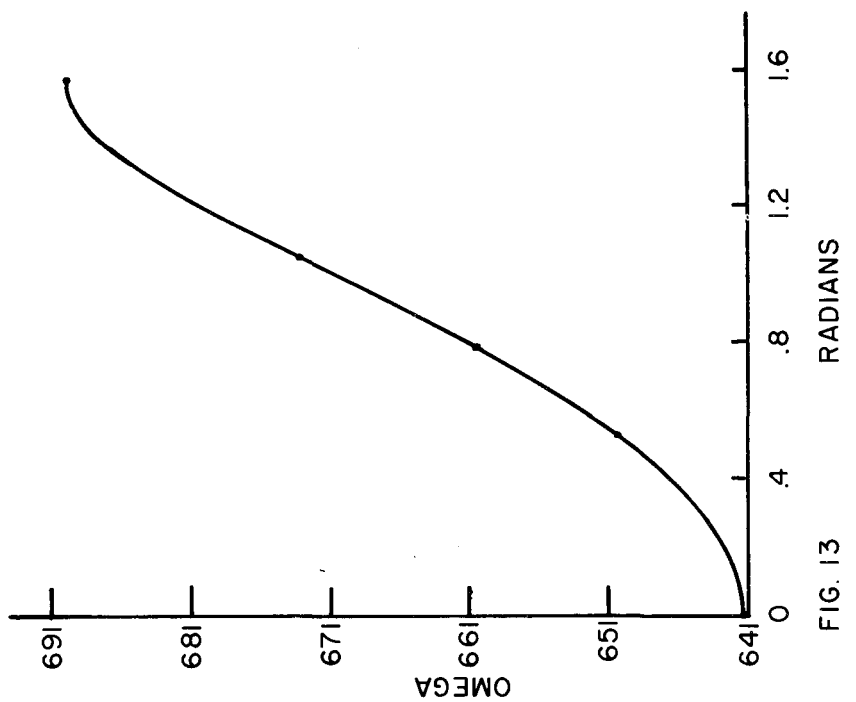
OMEGA
691
681
671
661
651
641
0
.4
.8
1.2
1.6
RADIANS

FIG. 13

calculations have been checked at two points with single cell cloverleaf cavities, and the quantities measured agree with calculated values quite well.

COUPLING STUDIES

The coupled circuit theory has been used extensively to analyze the behavior of the cloverleaf as far as its dispersion curve, tuning sensitivity, phase shifts and other electrical behaviors are concerned. It should be clear that the coupled circuits of two kinds with frequencies ω_1 and ω_2 certainly approximate the cloverleaf, with frequencies ω_1 associated with the cavities and ω_2 associated with the slots. Figure 13 shows a dispersion curve fitted to five data points taken from the demountable cloverleaf model. In this case, the cavity was capacitively loaded so that π mode frequency was 690 Mc/sec. This is a five-point fit to a three-parameter function (ω_1, ω_2, K); the maximum deviation of any point from the fitted curve is 28 kc which is only a little larger than measurement accuracy (full Q width at 3 db = 50 kc). We would thus say the theory fits the performance of this cloverleaf model exceedingly well. Many other model configurations have been fit and almost all agree this well with the theory. The upper branch of the passband may also be observed, and although the fit is no longer as good if these data points are included, indications are that the theory does adequately describe the observations. Fits with deviations to about 1 Mc are observed for this procedure. The presence of higher cavity modes not orthogonal to the slot mode, which couples the cavities in the TM_{010} mode, can effectively change the position of the upper branch somewhat. Figure 14 shows a fit of this type. In this case, the data are the same as in Fig. 13, but the slot mode points have been included. If ω_{cavity} is greater than ω_{slot}, the relative positions of the passbands are reversed and the structure becomes a backward wave device. Figure 15 illustrates this.

The important parameter as far as coupling is concerned is the effective bandwidth k_{eff} defined previously. As was mentioned this parameter enters strongly in the mode separation, phase shifts, and flattening sensitivity of the structure. Figure 16 shows a plot of k_{eff} vs slot length and width for the demountable cloverleaf, this time with no capacitive loading. The π mode frequency is 840 Mc. This curve is derived from the dispersion curve data points by fitting these points to the theoretical expressions to obtain K, ω_1 and ω_2, and then calculating k_{eff} from these parameters. It is found that the parameter K, yielding the coupling from slot to cavity, is virtually independent of slot configuration. This might be expected since the slot is very tightly coupled to the cavity fields, almost independent of its dimensions. With this information, it is clear from the figure that the effective coupling

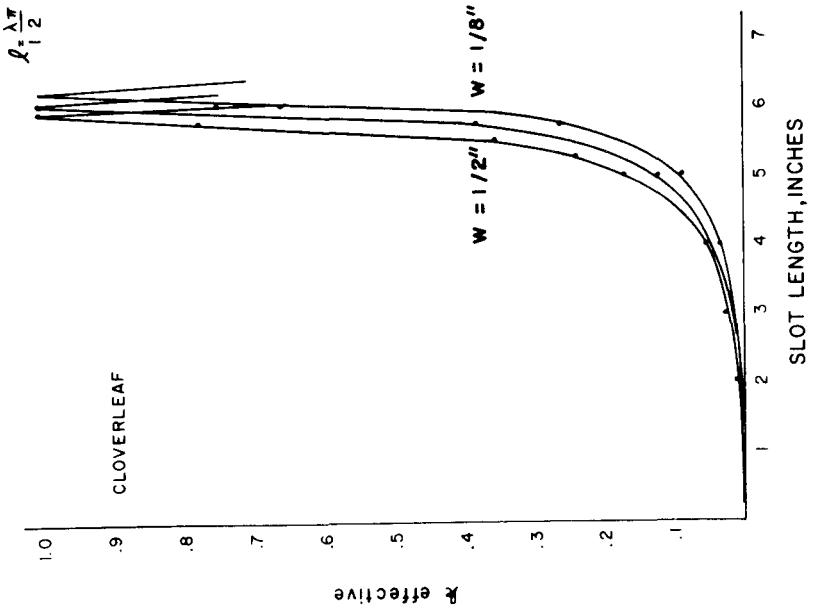
$\ell = \frac{\lambda\pi}{1\,2}$
W = 1/8"
W = 1/2"
CLOVERLEAF
SLOT LENGTH, INCHES
k effective
1.0
.9
.8
.7
.6
.5
.4
.3
.2
.1
1
2
3
4
5
6
7

FIG. 16

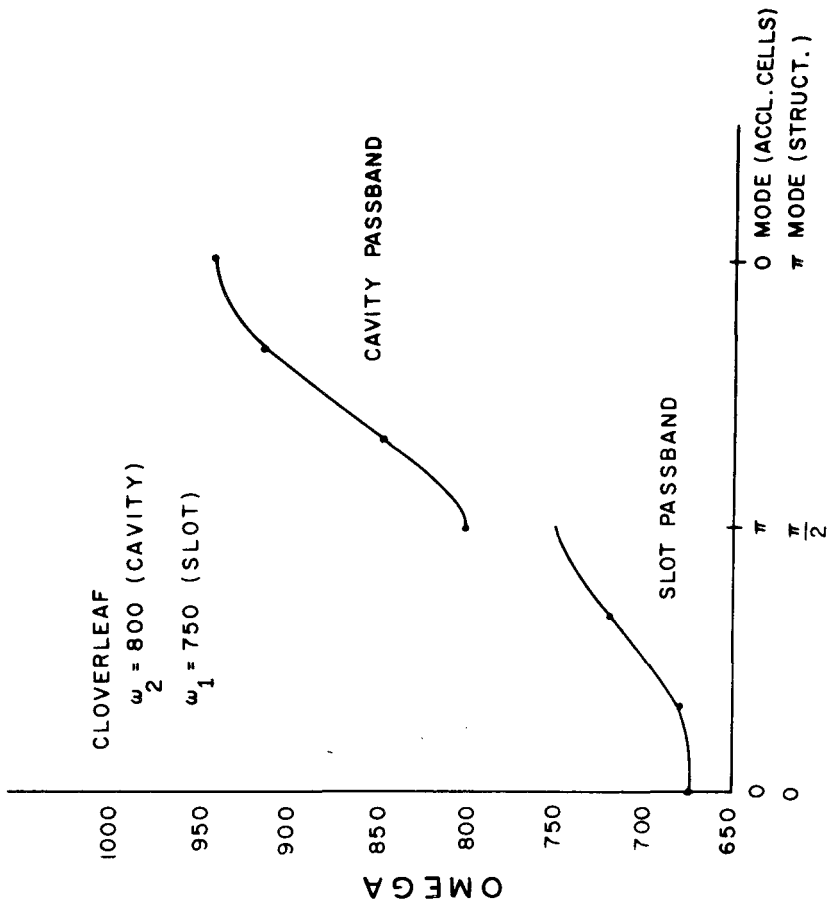
CLOVERLEAF
ω_2 = 800 (CAVITY)
ω_1 = 750 (SLOT)
CAVITY PASSBAND
SLOT PASSBAND
0 MODE (ACCL. CELLS)
π MODE (STRUCT.)
OMEGA
1000
950
900
850
800
750
700
650
0
0
π/2
π

FIG. 15

depends almost entirely on the resonant frequency of the slot. The dependence on width appears only as a change in resonant frequency with length (the effective length of the slot being somewhat longer than the actual length, the wider the slot the longer the effective length). At the slot length where the cavity frequency and the slot frequency are equal $k_{eff} = 1$, there are no phase shifts down the system, and the structure behaves as a $\pi/2$ mode structure as far as flattening and stability are concerned. It might be noted at this juncture that at resonance the slots should not have any appreciable electric field present, for a $\pi/2$ mode structure stores no energy in alternate cells in standing wave operation. For slot lengths giving resonant frequencies higher than the cavity frequency, very reasonable effective coupling constants may be obtained. Computer studies indicate very loose tolerance requirements are necessary on slot dimensions in order to get satisfactory performance. Even at resonance, variations of several megacycles in slot resonant frequency (like 0.025" in slot length) should have virtually no effect on performance.

As the accelerating cells get shorter, we should expect K to increase, yielding somewhat higher k_{eff} for the same slot length at lower energies.

Optimization of Shunt Impedance

The equation for shunt impedance may be written

$$ZT^2 = \frac{\left(\int E(z,t)\,dz\right)^2}{P\,L} = \frac{\left(n\int_0^{\ell} E(z)\sin\frac{\pi z}{\ell}\,dz\right)^2 Q}{\omega U\, n\ell}$$

where $Q = \frac{\omega U}{P}$, U = total stored energy in cavity, ℓ = cell length, L = cavity length, $n\ell = L$. The quantity ZT^2/Q may be evaluated using standard perturbation techniques (1). For a spherical metallic bead of radius r_o on the axis of a cavity of the type considered,

$$\frac{ZT^2}{Q} = \frac{\left(\int \left(\frac{\Delta f}{f}\right)^{1/2} \sin\frac{\pi z}{\ell}\,dz\right)^2 n}{\epsilon_o\,\pi\, r_o^3\,\omega} \qquad (11)$$

where $\frac{\Delta f}{f}$ = fractional resonant frequency shift produced at position z. It should be noted that this quantity is dependent upon geometrical factors only; losses in the cavity walls do not enter the expression. From a practical point of view, this means that errors in the values of ZT^2/Q

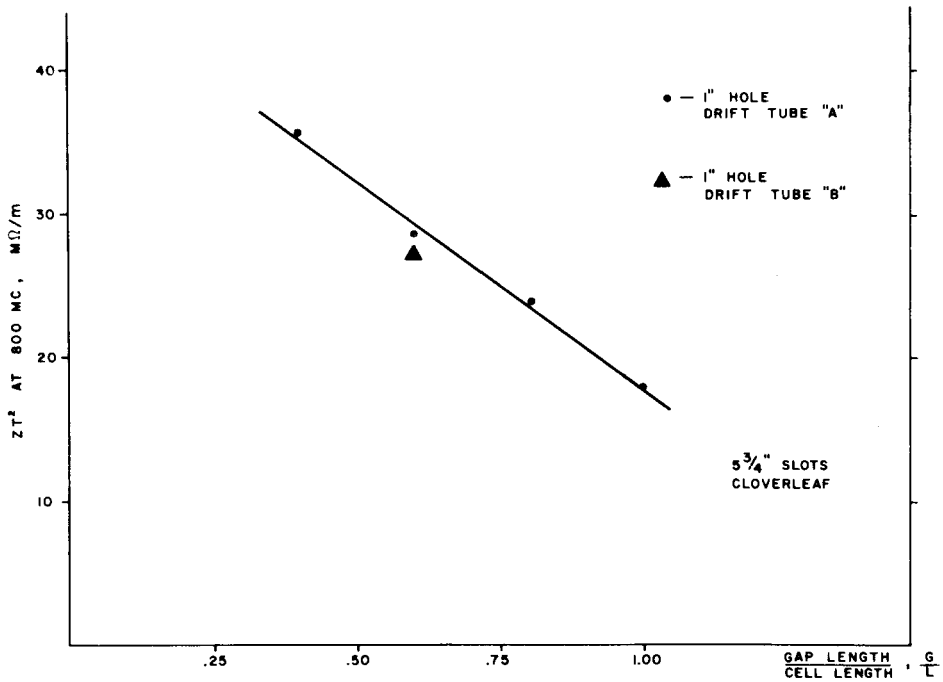

FIG. 17

VARIATION OF SHUNT IMPEDANCE WITH DRIFT TUBE PARAMETERS

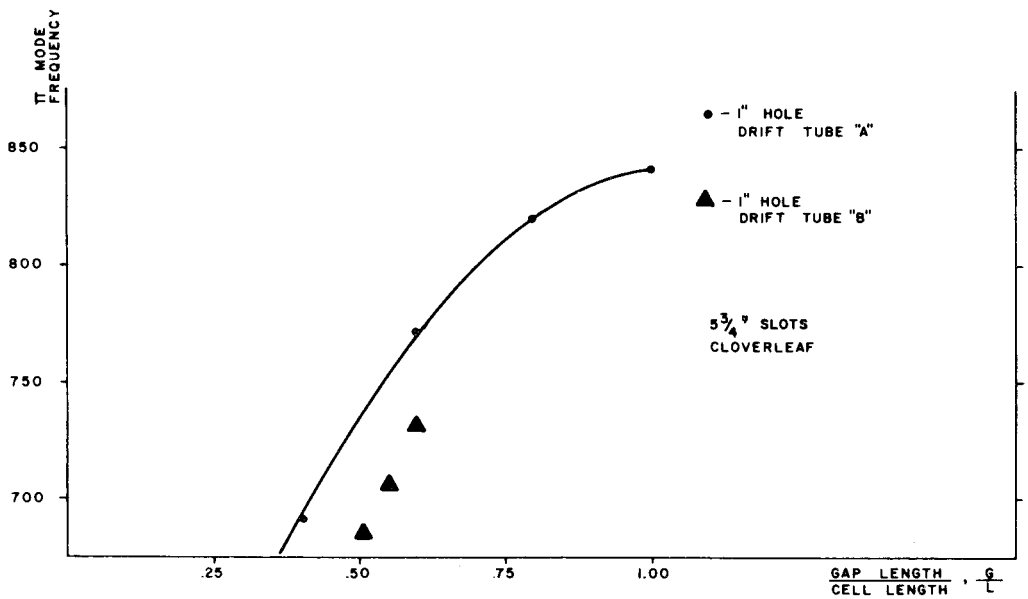

VARIATION OF π MODE FREQUENCY WITH DRIFT TUBE PARAMETERS

FIG. 18

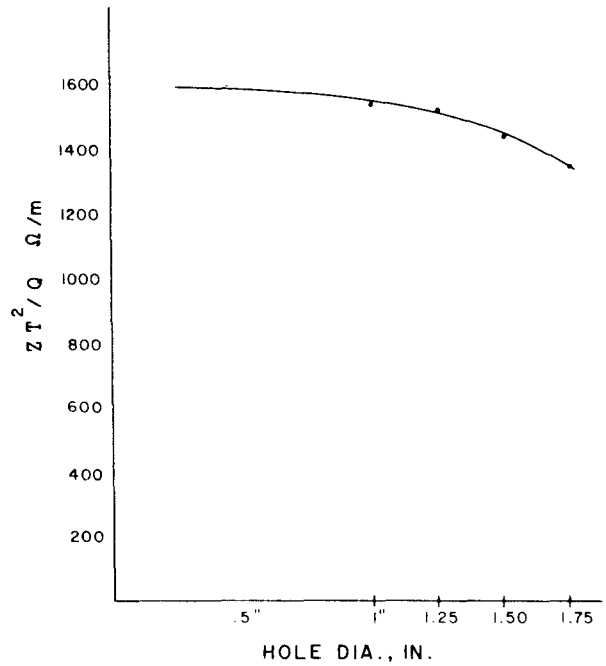
1600
1400
1200
1000
800
600
400
200
ZT^2/Q Ω/m
.5"
1"
1.25
1.50
1.75
HOLE DIA., IN.

FIG. 19

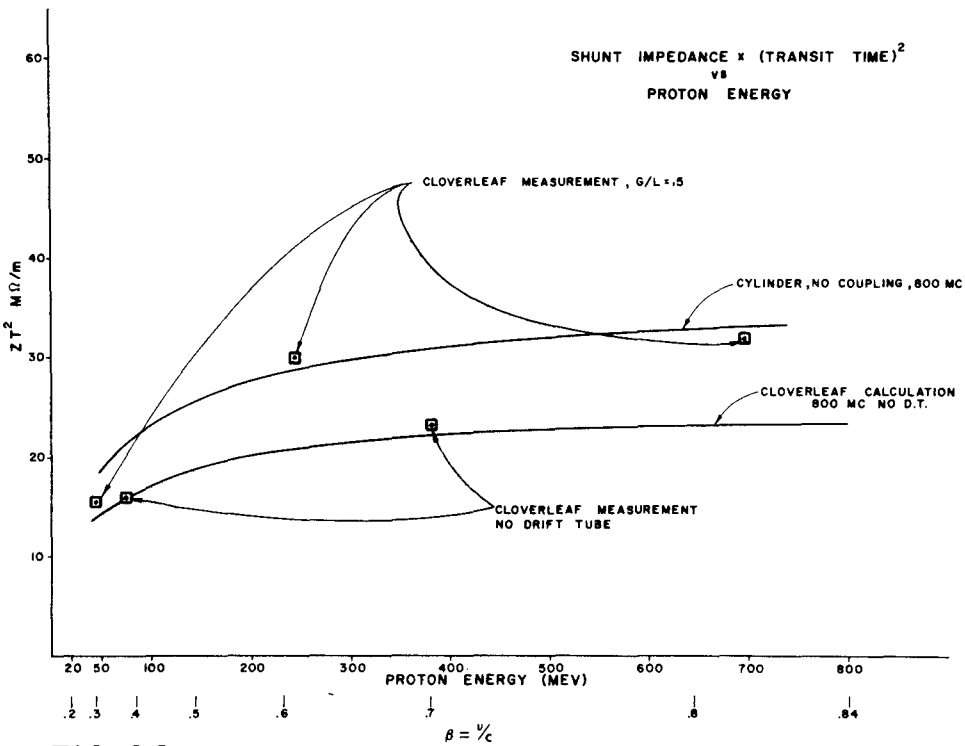
SHUNT IMPEDANCE x (TRANSIT TIME)^2
vs
PROTON ENERGY
CLOVERLEAF MEASUREMENT, G/L=.5
CYLINDER, NO COUPLING, 800 MC
CLOVERLEAF CALCULATION
800 MC NO D.T.
CLOVERLEAF MEASUREMENT
NO DRIFT TUBE
60
50
40
30
20
10
ZT^2 MΩ/m
20 50 100 200 300 400 500 600 700 800
PROTON ENERGY (MEV)
.2 .3 .4 .5 .6 .7 .8 .84
β = v/c

FIG. 20

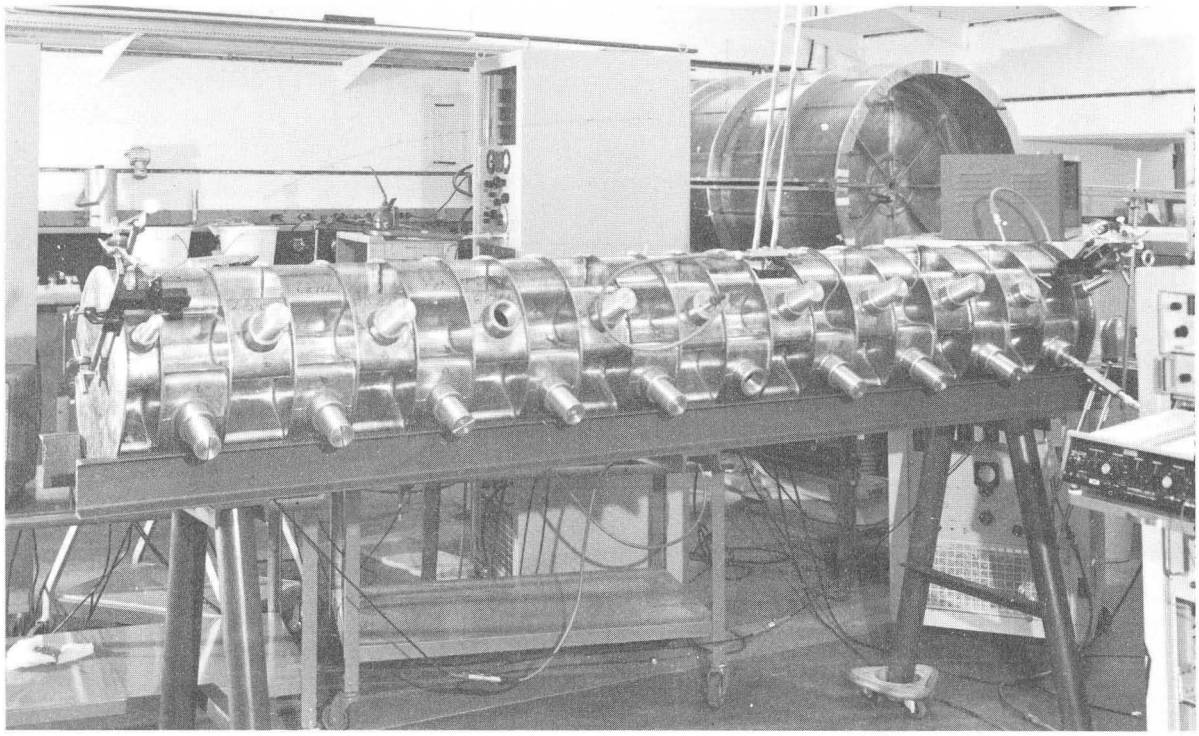

FIG. 21

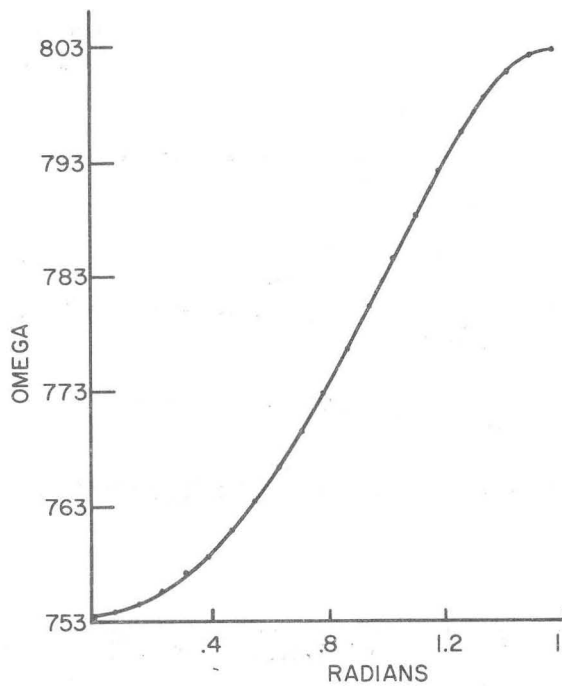

FIG. 22 21 Cell Air Model Cloverleaf Axial Field Flat To 1 Per Cent

obtained with demountable models are not dependent to any great extent upon the quality of the current joints attainable, and a relatively great trust may be placed in values obtained in somewhat crude models. However, to determine the effective shunt impedance accurately, an accurate determination of Q as well as ZT^2/Q is necessary. This is not a trivial problem, for the Q of a cavity depends very critically on the quality of the current joints in that cavity. Great pains have been taken to make high quality current joints in the demountable models tested, and even then variations on the order of 10% may be observed from one assembly to the next for identical configurations. In general, we can say that the values of ZT^2 quoted are lower than those realizable in cavities with all brazed joints, perhaps as much as 10% low. Q has been measured by measuring the power transmitted through a cavity as a function of frequency. With a highly undercoupled situation (small coupling loops) the frequency width of the half power points yields Q directly.

$$\left(\frac{\Delta f}{f}\right)_{1/2 \text{ power}} = \frac{1}{Q}$$

Other methods have been used, but this is the simplest and is accurate enough for the measurements we wish to make.

Variation of Shunt Impedance with Drift Tube Parameters

A reasonable way to increase the shunt impedance of the cloverleaf structure is to add drift tubes to the center of the septum walls in order to increase the transit time factor T^2 and to concentrate the stored energy in the cavity near the axis, effectively increasing Z/Q as well as T^2. Measurements have been made on the demountable model for two different shaped drift tubes. Figure 17 shows the variation of shunt impedance observed with g/ℓ (the ratio of gap length to cell length) for a 1" beam aperture. These results have been scaled to 800 Mc. Figure 18 shows the variation of π mode frequency. Figure 19 shows the variation of shunt impedance with hole size for $g/\ell = 0.6$. It is apparent that a large improvement in shunt impedance may be produced with the addition of drift tubes to the structure.

Several models with formed walls and all brazed construction have been fabricated to get reliable values of Q and ZT^2 for geometries which might be considered as elements in an accelerator. These models show Q's within 5% of theoretical for geometries where calculations are available.

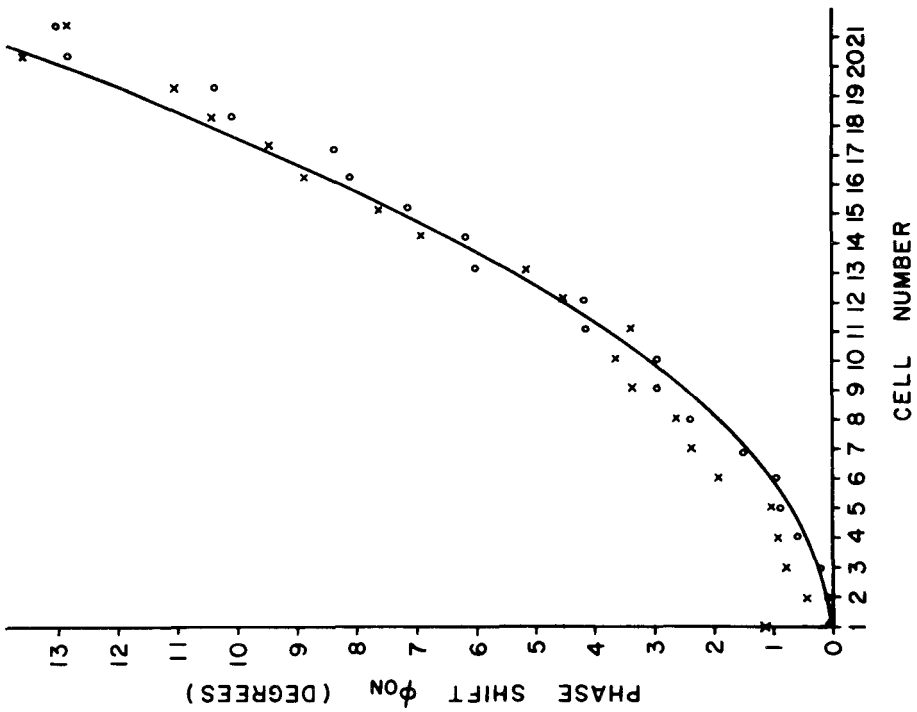
PHASE SHIFT ϕ_{ON} (DEGREES)
0 1 2 3 4 5 6 7 8 9 10 11 12 13
CELL NUMBER
1 2 3 4 5 6 7 8 9 10 11 12 13 14 15 16 17 18 19 20 21

FIG. 24

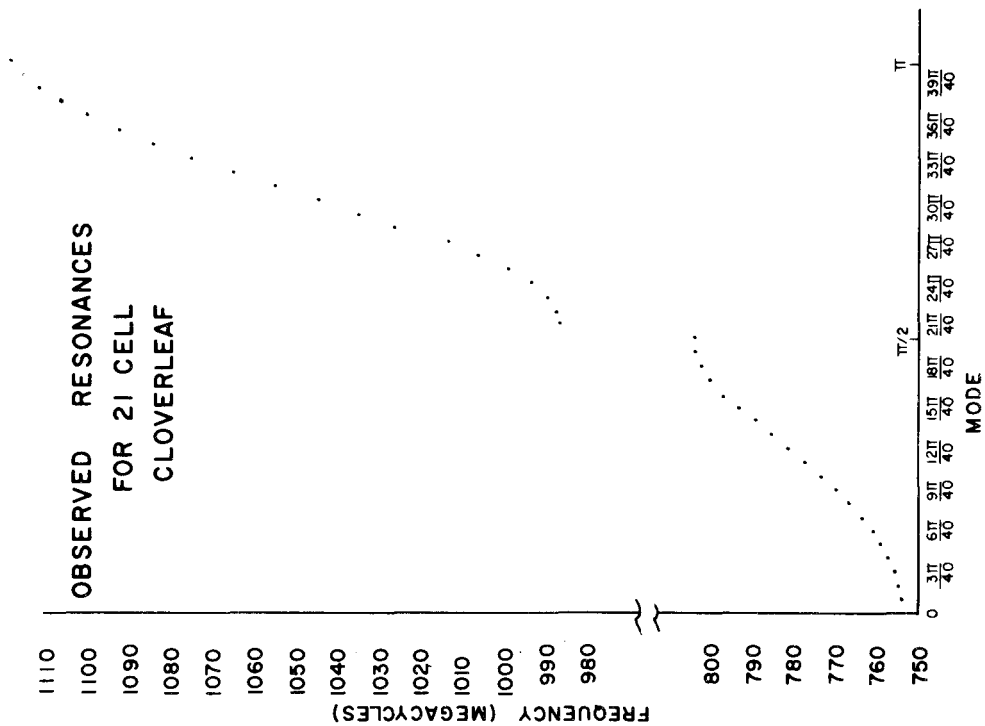
OBSERVED RESONANCES
FOR 21 CELL
CLOVERLEAF
FREQUENCY (MEGACYCLES)
1110 1100 1090 1080 1070 1060 1050 1040 1030 1020 1010 1000 990 980 800 790 780 770 760 750
MODE
0 3π/40 6π/40 9π/40 12π/40 15π/40 18π/40 21π/40 24π/40 27π/40 30π/40 33π/40 36π/40 39π/40 π/2 π

FIG. 23

A conservative set of parameters which we have investigated is:

g/λ	=	0.5
ω_{slot}	=	980 Mc (scaled from 840)
W_{π}	=	805 Mc/sec (scaled from 690)
k_{eff}	=	0.1042
L_{nose}/R	=	0.505
Hole size	=	1.25"
ZT^2	=	17 MΩ/m at β = 0.30 29 MΩ/m at β = 0.61 32 MΩ/m at β = 0.81

Figure 20 shows these data points plotted vs energy.

Higher values of shunt impedance could be obtained for various changes in the parameters above. It appears that decreasing g/λ will increase ZT^2 even more. Peak fields will set the limit for this change, and since no sparking measurements have yet been made, we do not feel justified in pushing this parameter. From dielectric bead measurements, we calculate peak fields on the drift tube surfaces of about 5 MV/m for 1 MV/m acceleration rate in the g/λ = 0.5 cavity at β = 0.6. This is certainly conservative. Flattening the ends of the noses will add a few per cent to the shunt impedance, but it is not felt worthwhile at this time.

21-Cell Prototype Model

Using approximately the above parameters, (β = 0.68), a 21-cell cavity has been constructed using the bent sheet metal technique with brazed joints. Figure 21 shows this model set up in our laboratory. The dispersion curve for this model is shown in Fig. 22. This was taken after the tank was flattened to about 1% in E. All points on this curve fit the calculated curve to better than 300 kc, the average error being about 75 kc. Figure 23 shows this dispersion curve with both passbands indicated. Analysis of these data gives an effective coupling k = 0.94, ω_1 = 803, and ω_2 = 934 Mc/sec.

The power flow phase shift has been measured in this model with the tank driven at one end (equivalent to a 40-cell tank driven in the middle). Figure 24 shows the measured values of phase shift along with the theoretical value given by

$$\Delta\phi_{n,o} = \frac{1 - k_{eff}}{k_{eff}\, Q} \quad n^2$$

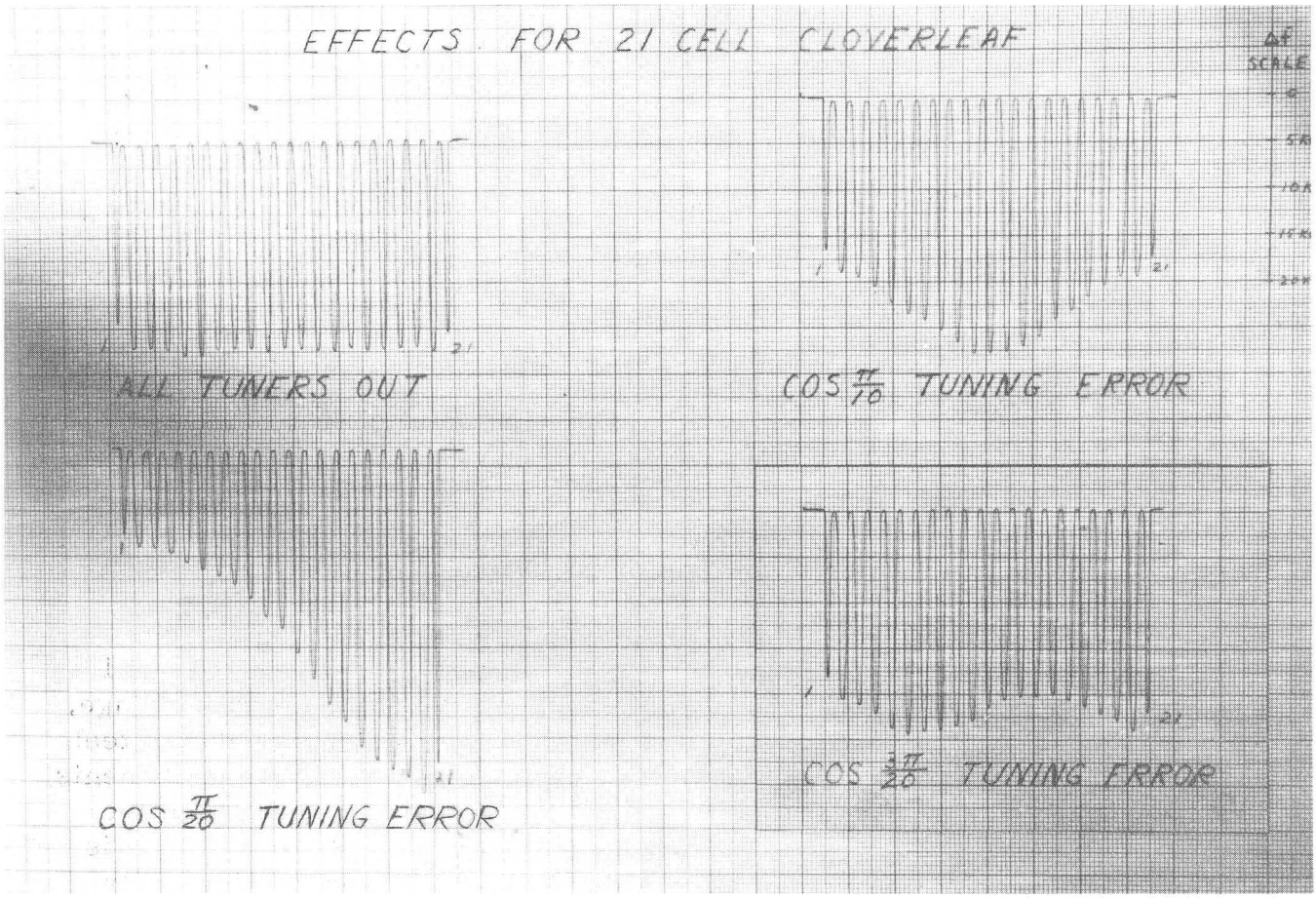
EFFECTS FOR 21 CELL CLOVERLEAF
ΔE SCALE
ALL TUNERS OUT
COS π/10 TUNING ERROR
COS π/20 TUNING ERROR
COS 3π/20 TUNING ERROR

FIG. 25

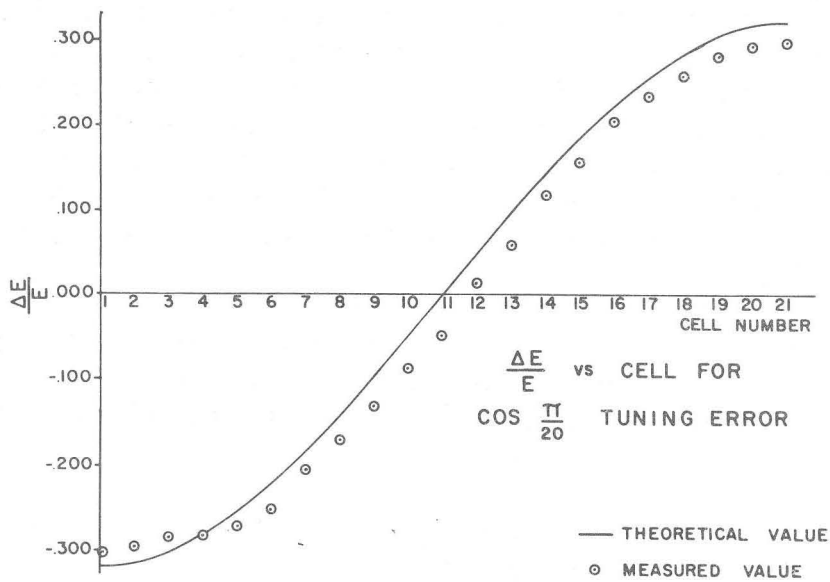
.300
.200
.100
.000
-.100
-.200
-.300
ΔE/E
1 2 3 4 5 6 7 8 9 10 11 12 13 14 15 16 17 18 19 20 21
CELL NUMBER
ΔE/E vs CELL FOR
COS π/20 TUNING ERROR
THEORETICAL VALUE
MEASURED VALUE

FIG. 26

where n is the number of cells downstream (away from the power source) from the cell in question.

The agreement between our theoretical expressions and the model measurements seems quite good.

For a π mode structure with effective coupling k we have the perturbation expression

$$\frac{\delta I_n^N}{I_n^N} = \frac{1}{k_{eff}} \sum_{r=1}^{N} \tilde{\epsilon}_r \frac{\cos \frac{\pi r n}{N}}{1 - \cos \frac{\pi r}{N}} .$$

If we introduce a tuning error $\frac{\delta \omega_n}{\omega_o} = a \cos \frac{\pi n p}{N}$ into our tank, we may check the predictions of the perturbation theory with the observed changes in field level in the tank. We have done this for p = 1, 2, and 3. Figure 25 shows the data for these measurements. A bead was pulled along the cavity axis at a constant rate, and the resonant frequency of the cavity scaled on a fast scaler. Frequency differences were recorded using a digital-to-analog converter; they were plotted directly by a x-y plotter, providing the records shown in the figure. The amplitude error induced may then be compared to the predictions of the perturbation theory. Figures 26, 27 and 28 show the comparison between the theoretical curves and the experimental points measured. Agreement seems quite good. From experience gained in flattening this prototype it appears that wall deformation will be adequate for tuning; no tuners should be required. Shunt impedance measurements indicate the same values quoted above for the shorter models.

Resonant Coupled Structures

Dunn, Sable and Thompson at Harwell were perhaps the first to point out some of the advantages of operating a structure with resonant coupling. The equivalent circuit theory used here allows even more advantages to be seen in the use of structures of this type. A resonant coupled π mode structure may be considered as a $\pi/2$ mode structure with cells of type 1 and 2 operating at the same resonant frequencies. Some properties of $\pi/2$ mode operation are

1. Every other cell (in this case the resonant coupling element) has no stored energy associated with it other than that required to transmit power to make up losses. This can be seen directly from the eigenfunctions of the chain

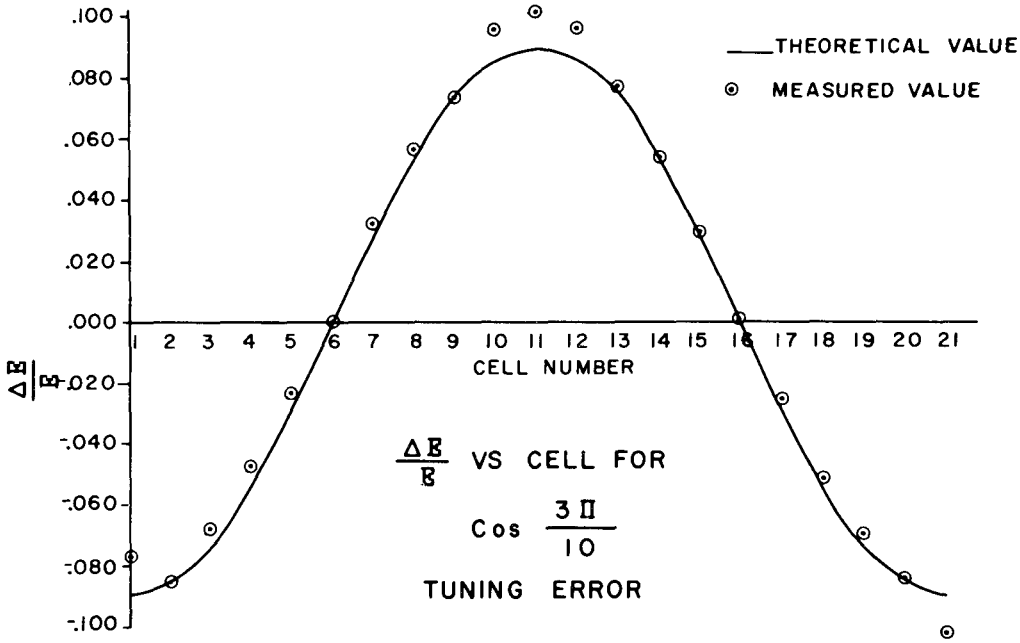
.100
.080
.060
.040
.020
.000
-.020
-.040
-.060
-.080
-.100
1 2 3 4 5 6 7 8 9 10 11 12 13 14 15 16 17 18 19 20 21
CELL NUMBER
ΔE/E
THEORETICAL VALUE
MEASURED VALUE
ΔE/E VS CELL FOR
Cos 3Π/10
TUNING ERROR

FIG. 27

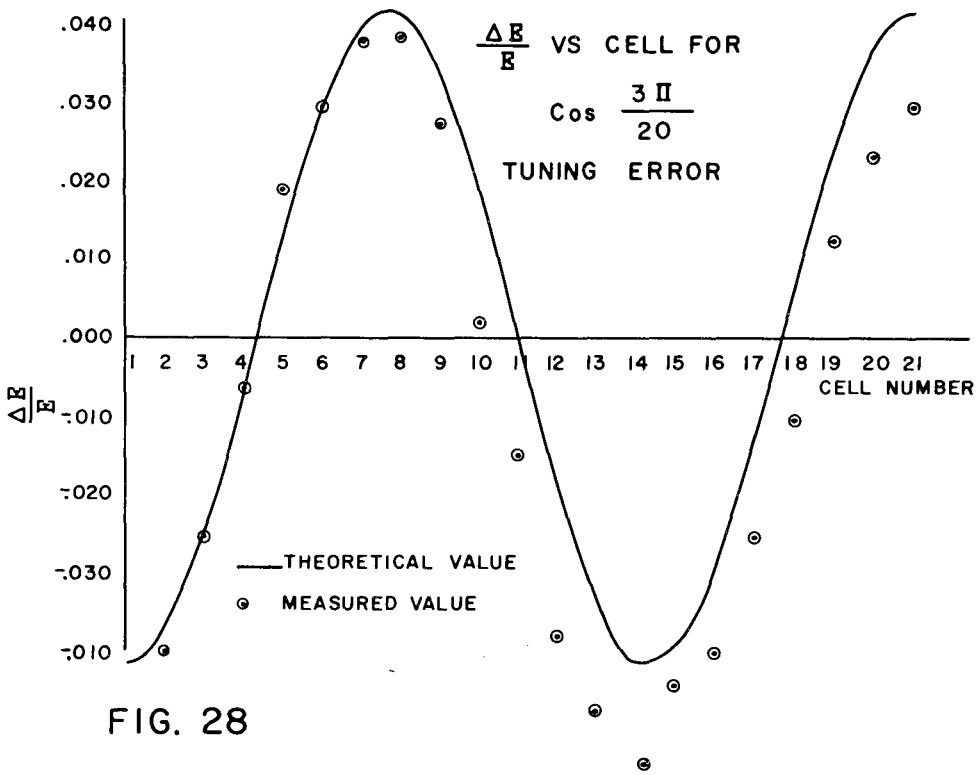
.040
.030
.020
.010
.000
-.010
-.020
-.030
-.010
1 2 3 4 5 6 7 8 9 10 11 12 13 14 15 16 17 18 19 20 21
CELL NUMBER
ΔE/E
ΔE/E VS CELL FOR
Cos 3Π/20
TUNING ERROR
THEORETICAL VALUE
MEASURED VALUE

FIG. 28

$$i_n^{N/2} = \cos \frac{\pi}{2} n .$$

Thus one should not have to worry about sparking in coupling elements, losses in coupling elements, etc.

2. The phase of all accelerating cells is locked at π, any variations occurring only through second-order effects in frequency errors. This may be seen by considering the circuit equation

$$X_{n+2} = -X_n + \frac{2}{k}\left(-\frac{2\Delta\omega_{n+1}}{\omega} + \frac{i\,\omega_n}{\omega Q}\right) X_{n+1}; \qquad (12)$$

if cell $n+1$ is a coupling cell, its amplitude is small (point 1) and imaginary (for power flow). The phase shift is then the product of two numbers which are small, $\frac{\Delta\omega_n}{\omega}$ and X_{n+1}. For no errors, we see no phase shift.

3. The amplitude of the fields in the accelerating cells is independent of frequency errors in any cells in first-order theory. Second-order effects do occur but only for very large amplitude errors. This may also be seen from Eq. (12), amplitude variations being the quotient X_{n+1}/Qk which is very small indeed. If X_{n+1} has a real component (due to other frequency errors in accelerating cells), then some amplitude variation may take place due to coupling cell mistunings, but the sensitivity is very low.

4. From Eq. (12), if X_{n+2}, X_n are coupling cell amplitudes and X_{n+1} an accelerating cell amplitude, we see that as $\Delta\omega_{n+1}$ goes through zero we should see a minimum in the coupling cell field X_n. This provides an exceedingly easy way to tune a structure of this type, for now one can choose a frequency, and successfully tune coupling cell fields to minima by changing accelerating cell tuners, working from a point furthest from the drive point toward the drive. It can thus be tuned, one cell at a time, to any predetermined frequency.

5. Since operation is now at the center of the passband where the slope is steepest, mode separation is maximum, and considerably narrower bandwidth may be tolerated for satisfactory performance.

6. This allows us to separate the shunt impedance problem from the coupling problem to some extent and may allow better shunt impedance optimizations.

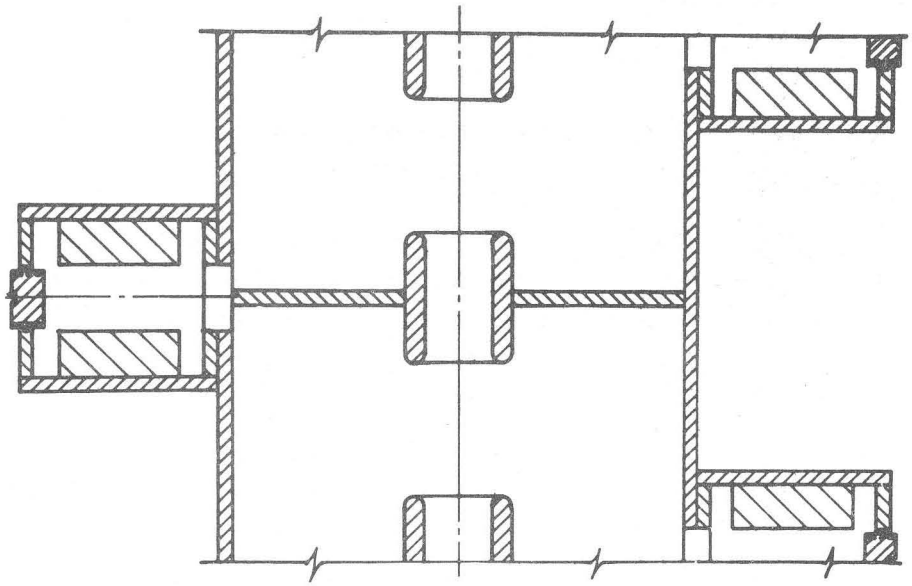

FIG. 29

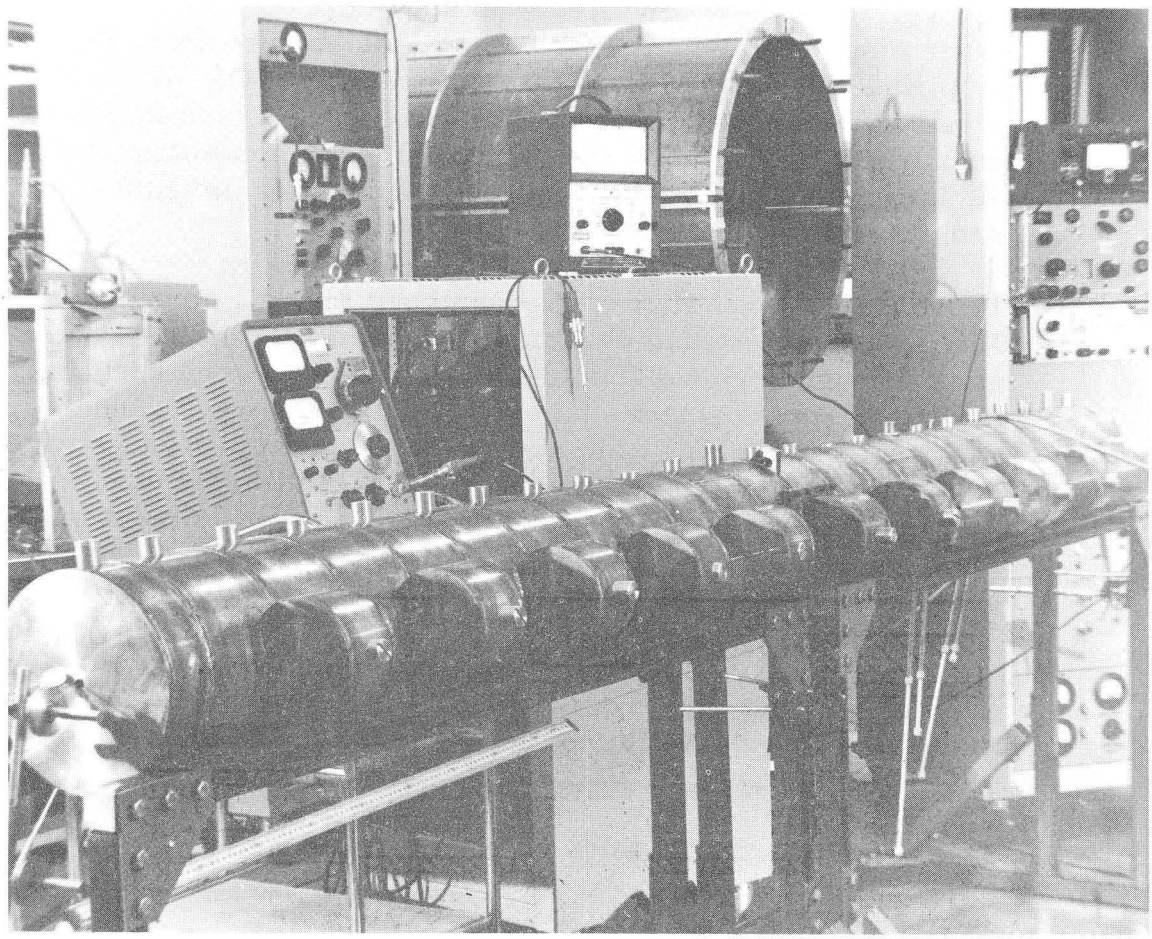

FIG. 30

We have built two models with resonant coupling devices and quite narrow bandwidths to investigate these properties. Figure 29 shows two accelerating cavities coupled by a side cavity which is resonant at the same frequency as the accelerating cavities. A slot cut in the mutual side walls of the cavities provides energy transfer from accelerating cell to coupling cell, etc. Since the coupling cell stores no energy in $\pi/2$ mode, its Q does not contribute to the shunt impedance values obtained, and thus this cavity may be made without too much regard to the Q obtained. We thus may heavily load the side cavity to make it small without affecting the shunt impedance appreciably. Since the slot which couples energy may be made quite small, one is free to modify the accelerating cavity at will in order to increase its shunt impedance. We have not tried to do this as yet. Figure 30 shows a photograph of a 24-cell model of a structure of this type. Shorter models have also been constructed of this configuration. After tuning up by the method described in point 4 above, a very reasonable dispersion curve is obtained near the $\pi/2$ mode with 1" x 2" slots. The structure shows a 20 Mc bandwidth at 810 Mc with 500 kc mode separation on either side of the $\pi/2$ mode. Near the zero and π modes, the Q curves overlap so badly no data are available.

In the limited time available before this meeting, we have seen no deviations from the predictions of the theory. When just tuned up, the tank was flat to $\sim \pm$ 5% in E, and we have not been able to change this with any reasonable tuning arrangement. Since construction of this tank was quite crude, we might expect geometrical errors to account for this. Measurement of field levels in coupling cells indicates negligible energy stored in them. No phase shift can be detected between one end and the other of the model. Detailed measurements and comparison with theory are under way and should be completed shortly. Shunt impedance values of 30 MΩ/m at $\beta = 0.7$ have been obtained with the models.

In closing I would like to note that the cloverleaf can also be run resonantly coupled. No field should develop in the slot for, as we have noted, alternate cells store no energy in the $\pi/2$ mode operation. This would make a structure which should be extremely stable.

Development work is continuing on these structures. We also hope to check sparking levels in a short cloverleaf cavity with 100 kw of pulsed rf at 805 Mc/sec soon.

CARNE: What was the Q of your 21-cell model?

KNAPP: The Q is about 16, 500.